



Thermochemical conversion of pulverized carbon carriers under super high heating rates and elevated pressures

Markus Bösenhofer^a, Thomas Nanz^b, Hugo Stocker^c, Christoph Feilmayr^d, Johannes Rieger^b, Michael Harasek^a

^a TU Wien, Institute of Chemical, Environmental and Bioscience Engineering, Getreidemarkt 9/166-2, Vienna, 1060, Vienna, Austria

^b K1-MET GmbH, Area 1 - Metallurgical Process Efficiency and Circularity, Stahlstraße 44, Linz, 4020, Upper Austria, Austria

^c voestalpine Stahl Donawitz GmbH, Kerpelystraße 199, Leoben, 8700, Styria, Austria

^d voestalpine Stahl GmbH, voestalpine-Straße 3, Linz, 4020, Upper Austria, Austria

ARTICLE INFO

Keywords:

Thermochemical conversion
High heating rate
Entrained flow reactor
Pulverized coal
Burnout
Pore formation
SEM analysis
Blast furnace simulation

ABSTRACT

Understanding the thermochemical conversion of pulverized carbon carriers under high heating rates is vital for improving efficiency and reducing emissions in high-temperature industrial processes. Three coal types (anthracitic, bituminous, and sub-bituminous) are investigated under high heating rates (up to 10^6 K/s) and elevated pressures (2 bar_(g)) using a novel pressurized entrained-flow reactor: the Alternative Reducing Agent (ARA) reactor capable to reproduce the intense thermal environment of blast furnaces.

Heating rate effects are isolated during the experiments to investigate the effect of the heating rate on the thermochemical conversion. Burnout ratios, ash content, and particle size distributions were assessed via the ash tracer method and laser diffraction analysis. Scanning Electron Microscopy (SEM) provided insights into morphological transformations.

The results demonstrate clear heating rate dependent conversion behavior. Burnout ratios increase with volatile content and are significantly higher in high heating rate and matching temperature experiments than in low heating rate experiments. Higher heating rates enhance coal reactivity, reduce char residue, and increase pore formation, particularly in bituminous and sub-bituminous coals. The anthracitic coal displayed less pore development and ash flake deposition. Matching temperature conditions yielded intermediate burnout levels but significantly more residue than the high heating rate cases, confirming the heating rate's impact on reactivity.

The ARA reactor's capability to provide high heating rate conditions under controlled settings offers a valuable platform to validate and improve simulation models and supports the development of more sustainable industrial processes.

1. Introduction

The thermochemical conversion of solid carbon carriers is important in many applications, e.g., coal or biomass boilers in electric power generation, blast furnaces for ironmaking, or rotary kilns in the high-temperature industry. A thorough understanding of the involved conversion processes is crucial for efficiency increases and emission reductions.

The thermochemical conversion process consists of the following sub-steps [1,2]:

- drying
- pyrolysis/devolatilization
- oxidation and gasification.

The physical sub-processes involved in these thermochemical steps are [3]:

- Mass and energy transfer between the bulk gas phase and the solid surface
- Intra-particle mass and energy transport between the particle size and reaction site
- Adsorption or desorption of the gaseous educts and products to or from the reaction site

The conversion conditions, e.g., temperature, pressure, heat and mass transfer rates, and gas phase composition, are decisive for the conversion rates [4–7]. Despite the importance of high heating rate

* Corresponding author.

E-mail address: markus.boesenhofer@tuwien.ac.at (M. Bösenhofer).

conversion conditions in industrial applications, the effects of the heating rate are not so well researched compared to the effects of species concentrations and temperature. A better understanding of high heating rate processes enables emission reductions with existing industrial equipment within a short time frame.

The injection of pulverized carbon carriers into the ironmaking blast furnaces raceway zone is an important example for high heating rate conversion [7] as around 60% and 70% of the steel is produced using the blast furnace route in the EU [8] and worldwide [9], respectively. In addition, around 50% of the reduction equipment currently installed is based on the conventional (carbon intense) route. While direct reduction technologies are yet to breakthrough, a better understanding of the injection process in the blast furnace enables emission reductions with existing equipment and within a short time frame throughout various industries.

In the blast furnace, particles are injected into the hot blast above the blast furnace hearth and experience intense heat transfer from the hot coke and hot blast. Direct experimental investigation of this injection process is challenging due to the harsh conditions. We implemented a novel pressurized entrained flow reactor to recreate those conditions [10,11] because existing test rigs failed to reproduce the required conditions [7,12]. The reactor design and the desired conversion conditions are based on the findings of our various simulation studies on thermochemical conversion in the blast furnace raceway zone [13–16].

In this work, we present the first results comparing high and low heating rate experiments at elevated pressures and discuss the experimental strategies to isolate the heating rate effect from other effects. In this context high heating rates refer to heating rates above 10^4 K/s, while low heating rates refer to below 10^4 K/s. Most experimental equipment struggles to provide heating rates above 10^4 K/s [7,17], therefore, investigating heating rate effects on the thermochemical conversion of solids is limited, especially under elevated pressures.

Experimental investigation of the effect of low ($<10^4$ K/s) and high ($>10^4$ K/s) heating rates on the thermochemical conversion of coals has been done by Li et al. [18,19] before. They used a drop-tube furnace (DTF) and an injection rig (IR) to reach high and super high heating rates, respectively and their results indicate different conversion characteristics for the different heating rates. Since the high and super high heating rate experiments have been conducted in different experimental setups, a device specific bias of the results cannot be excluded. Other than that, Kim et al. [20] investigated thermal stress induced particle fragmentation at high heating rates by comparing particle size distributions. However, no evaluation of the heating rate's effect has been done by them. Contrary, Yan et al. [21] compared the product yields of super low ($<10^1$ K/s), low (10^1 to 10^4 K/s), and high ($>10^4$ K/s) heating rates. Their results indicate a higher carbon mobilization at higher heating rates. To the best knowledge of the authors, only the works of Lie et al. [18,19] is comparable to the presented results. Furthermore, the presented experimental setup and results are the first to compare the thermochemical conversion under low and high heating rates obtained in single experimental setup. The novel experimental setup enables the investigation of heating rate effects avoiding reactor specific conversion biases and provides novel data to validate CFD models.

The following section introduces the entrained flow reactor, the experimental procedure and the investigated carbon carriers. This is followed by the discussion of the experimental results the summary and conclusions.

2. Materials and methods

2.1. Experimental setup

The experiments used the Alternative Reducing Agent (ARA) reactor of K1-MET located at and operated with TU Wien [10,11]. The ARA

reactor is an entrained pressurized flow reactor and was specifically designed to recreate the harsh conditions prevalent in the blast furnace raceway zone. These conditions are characterized by high heating rates, high temperatures, elevated pressures, and short residence times [7]. Table 1 compares typical raceway conditions and the ARA reactor operation conditions.

The main difference between the raceway zone and the ARA reactor is the flow regime. While turbulent flow dominates in the raceway, laminar to transitional flow occurs in the ARA. Furthermore, the absolute and relative gas and particle velocities are at least one order of magnitude lower in the ARA reactor. The Stokes number of $50\ \mu\text{m}$ particles in the injection region is around 4 and 0.9 in the raceway zone and the ARA reactor respectively.

The higher initial gas–particle relative velocity and the larger Stokes number cause higher convective heat fluxes in the raceway compared to the ARA. A hydrogen flame surrounds the injection point in the ARA reactor to compensate the smaller convective heat fluxes with radiative ones. This thermodynamic compensation of the fluid dynamics seems adequate because the Stokes number's influence on the thermochemical conversion are limited to the heat transfer rate and reaction conditions [7,16]. The exact heat transfer rate cannot be determined experimentally, but will be evaluated by detailed Computational Fluid Dynamic (CFD) simulations. A preliminary CFD study of the reactor and representative particle heating rates was presented elsewhere [22,23]. The heating rates were also confirmed by a simple heat balance model based on the experimentally measured temperatures.

The hydrogen burner was developed by Andritz FBB GmbH and is a non-premixed burner. Hydrogen and oxidizer (air) are introduced through co-axial lances surrounding the coal lance. Ten small nozzles each adjust the hydrogen and air flow to form a toroidal flame surrounding the injection lance. The burner operates in autoignition mode and ignites at the refractory surface. The particles are injected through the center hole of the burner lance and fed to the system via a revolver doser [24]. A rotating disk is transporting coal particles to the carrier gas stream from a slightly fluidized bed. Pre-heated co-flow and particles mix in the burner and react through out the reaction zone inside a ceramic pipe with sixteen sample ports. After the reaction zone, the gas–particle mixture is quenched and diluted with nitrogen before the solid residues are separated in the cyclone. Fine particles are subsequently removed via a filter before the flow rate is determined by an orifice. The pressure retaining valve releases the system pressure and enables subsequent gas sampling for the gas analyzer and gas chromatograph (GC). Fig. 1 shows the main components of the ARA reactor.

The ARA reactor was designed for a constant particle mass flow of around 1–2 g/min, which is injected to a co-flow of at least $20\ \text{Nm}^3/\text{h}$. Assuming a coal density of $1300\ \text{kg}/\text{m}^3$, the volume share of the coal particles is below $10^{-5}\ \text{m}^3/\text{m}^3$, which theoretically ensures single particle conversion characteristics. However, there is currently no possibility to verify the particle distribution in the reactions zone.

Preliminary CFD studies indicate some temperature stratification along the axial and radial direction. The results have not been validated yet, therefore, we have to assume uniform conditions for the subsequent investigations. Furthermore, the expected heating rates can currently also only be estimated from energy balances.

The ARA reactor can be operated with and without the hydrogen burner being active to investigate the influence of high heating rates on thermochemical carbon carrier conversion. This work uses different reactor operation modes and experimental settings to isolate the effect of heating rate on coal conversion. In other words, particles are converted at similar effective conditions but the initial heating rate at particle injection is altered. A thorough fluid dynamic investigation to obtain detailed reactor states is ongoing, while first results using a simplified model to investigate particle conversion conditions have been published [22,23].

The ARA reactor combines the characteristic features of drop tube furnaces, entrained flow reactors, and injection rigs [7] and provides unique experimental possibilities. Heating rates above 10^4 K/s at elevated pressures have not been reported in literature so far [7,17].

Table 1
Comparison of typical raceway conditions and the ARA reactor operation conditions [7,10].

	Temperature (°C)	Heating rate (K/s)	Pressure (kPa _(a))	Gas velocity (m/s)	Particle velocity (m/s)	Residence time (ms)	O ₂ content (vol%)
Raceway	1200–2300	10 ⁴ –10 ⁶	200–500	200	20	20–100	~27
ARA	<1800	10 ⁴ –10 ⁶	100–800	4–30	1–2	50–200	<25

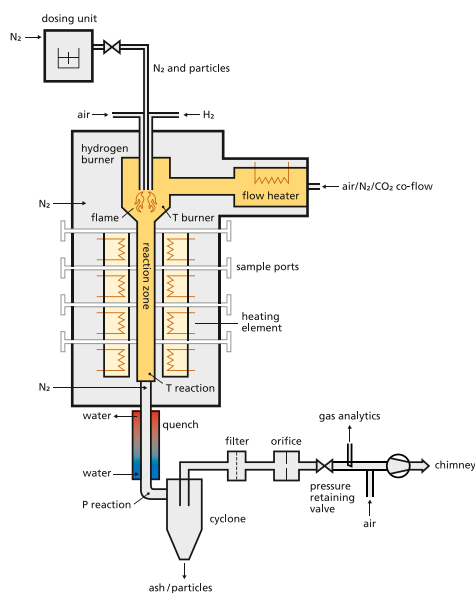


Fig. 1. Schematic overview of the ARA Reactor [10,11] (© K1-MET GmbH, TU Wien).

2.2. Experimental procedure

The experimental campaign aims to identify conditions which enable the isolation of heating rate effects to investigate heating rate effects on thermochemical coal conversion. Therefore, a set of experiments under specific conditions is performed. Three different experimental conditions were investigated for each of the different coals. They are subsequently called: (i) hydrogen burner (HB), (ii) no burner (NB), and (iii) matching temperature (MT).

The hydrogen burner is active at 2 Nm³/h fuel rate in the HB experiments, while the burner is off in the NB ones. During the MT experiments, the flow rates were similar to the NB conditions, except that the heating elements were set to match the outlet temperature T_{reaction} of the HB cases. The expected heating rates are calculated using an energy balance approach for 50 μm particles. Table 2 summarizes the experimental conditions.

The general experimental procedure consists of a pre-heat phase, where the ARA reactor is heated to the required temperature, and a pressure charging step to reach the experimental pressure. After the experimental settings are reached and stable, the dosing unit is prepared, and the actual experiment starts with the solid dosing. The carbon dioxide content in the off-gas is used to monitor the dosing stability and the experiment is stopped when the carbon dioxide concentration drops towards ambient values, which indicates a dosing rate decrease. Axial temperature gradients inside the reaction zone are minimized by four independent heating zones, which was also confirmed by preliminary CFD simulations [14].

The solid residues captured by the cyclone are discharged from the reservoir, and the next experiment is prepared. A typical experiment lasts around 40 min and the sample exchange time is approximately 15 min. The sampling procedure is tedious when discharging the particles from the test rig. Despite rigorous measures, cross-contamination between subsequent/preceding samples cannot be fully eliminated. We

Table 2
Experimental conditions of the different experimental settings.

	HB	NB	MT
Co-flow (Nm ³ /h)	50 ± 1.2	50 ± 1.2	50 ± 1.1
Air flow (Nm ³ /h)	5 ± 0.08	5 ± 0.07	5 ± 0.08
Hydrogen flow (Nm ³ /h)	2 ± 0.06	–	–
Carrier flow ^a (Nm ³ /h)	1.5–2	1.5–2	1.5–2
Equivalence ratio (–)	1	–	–
Coal mass flow ^a (g/min)	0.8–1.8	0.8–1.9	1.8–3.0
Co-flow temperature (°C)	1075 ± 3	1075 ± 16	1075 ± 8
Heater temperature (°C)	800 ± 10	800 ± 8	1300 ± 12
Expected heating rates (K/s)	1.2·10 ⁵	3.4·10 ⁴	6.9·10 ⁴
pressure (kPa _(g))	220 ± 8	220 ± 8	220 ± 7

^a depending on coal type

Table 3
Proximate analysis and particle size information of the tested coals.

	Coal A	Coal B	Coal C
C (% _w d)	80.30	78.32	72.98
C _{fix} (% _w d)	77.21	65.45	58.34
volatiles (% _w d)	11.99	23.35	32.36
ash content (% _w d)	10.52	9.95	10.05
moisture content (% _w ar)	1.12	1.25	1.17
d ₁₀ (μm)	3.62	5.01	5.04
d ₅₀ (μm)	28.53	44.18	40.63
d ₉₀ (μm)	254.79	245.77	143.54

d ... dry, ar ... as received

aim to collect significant sample mass (>10 g) for each experiment to ensure meaningful results.

2.3. Coal samples

The thermochemical conversion of three different coals is investigated in this work: an anthracitic (coal A), a bituminous (coal B), and a sub-bituminous (coal C) coal. Table 3 gives the investigated coals' proximate analysis and particle size information.

The coals were milled to particle sizes below 300 μm with a mean diameter between 25 and 45 μm . The particle size distribution was determined in the Mastersizer 2000 using approximately 1 g sample. The particle size distribution (PSD) and particle size sum (PSS) of the virgin coal samples are shown in Figs 3, 4, and 5. Coal A and B feature a bimodal PSD, while coal C features a monomodal distribution. With the aforementioned 1 to 2 g/min coal flow rate, approximately 60 to 70 g of coal were consumed in typical trail lasting approximately 1 h.

3. Experimental results

3.1. Particle burnout

The particle burnout ratio (BO) is calculated using the ash tracer method [25,26]:

$$\eta = \frac{10^4 (Y_{\text{ash}} - Y_{\text{ash},0})}{Y_{\text{ash}} (100 - Y_{\text{ash},0})} \quad (1)$$

where $Y_{\text{ash},0}$ and Y_{ash} are the virgin coal and residual char ash mass fraction on a dry basis, respectively.

The ash content of the samples was determined via TGA following the DIN 51734/51719, except for the sample mass, which was in the

Table 4
Experimental ash content, burnout ratios, and solid residue yield.

	HB			NB			MT		
	ash content (% _{wf})	burnout ratio (-)	solid residue (% _{wf})	ash content (% _{wf})	burnout ratio (-)	solid residue (% _{wf})	ash content (% _{wf})	burnout ratio (-)	solid residue (% _{wf})
Coal A	16.84	0.491 ± 0.25	26.9	12.53	0.179 ± 0.37	65.0	18.77	0.419 ± 0.27	35.3
Coal B	23.66	0.664 ± 0.18	14.0	14.81	0.364 ± 0.28	59.8	22.14	0.611 ± 0.18	23.9
Coal C	52.16	0.898 ± 0.07	3.8	27.89	0.711 ± 0.14	19.0	50.18	0.889 ± 0.08	9.5

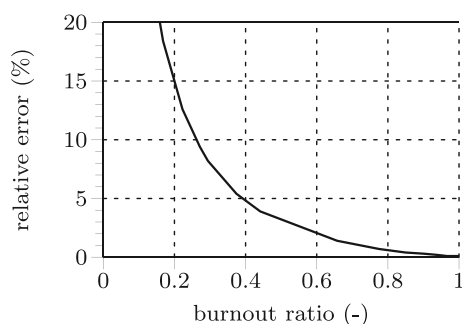


Fig. 2. Relative error of the burnout depending on the burnout.

order of tenths of mg instead of one gram. The dried sample is heated to 500 °C within 60 min and subsequently heated to 815 °C, where the sample is kept for 60 min before being cooled down to ambient temperature. The TGA mass loss curves were used to determine the ash content and, subsequently, calculate the burnout ratios.

The uncertainty in determining the ash content leads to a larger uncertainty for the burnout at lower burnouts. As the difference between the ash content of the raw and burnt coal increases, the error gets smaller. DIN 51719 states describes a repeatability limit of 0.2 w% abs. for an ash content lower than 10% and 2% rel. otherwise. The ash contents of the original coal and the burnt residues were adapted by their corresponding repeatability limits to calculate the error of the derived burnout. Fig. 2 shows the error versus the coal burnout.

Table 4 summarizes the determined ash contents, burnout ratios, and the solid residue amount of the different coals for the three experimental conditions.

The burnout ratios indicate a slower conversion of coal A and B compared to coal C under all conditions, and they increase according to the volatile content. Furthermore, the HB and MT cases show similar burnout ratios for all coals, while the NB case results in significantly lower burnout ratios. The burnout reduces by approximately 50% for coal A and B and by approximately 20% in the NB experiments compared to the other experiments. The different burnout ratio changes indicate a higher temperature dependence of the coal A and B conversion characteristics. These findings are also present when comparing the sample mass collected in the cyclone to the dosed coal mass (solid residue share). However, a significant difference exists in the solid residue share: the recovered solid mass is higher for the MT experiments for all coals. This effect indicates some influence of the burner on the conversion process.

The lower residue yield of the HB case is most likely caused by the higher reactivity of the coal char due to higher heating rates compared to the MT case [4,27]. According to Thomas et al. [4], the reactive fraction of the coal maceral inertinite increases at high heating rates and, thus, increases the reactivity of coal char. Furthermore, according to Liu et al. [27], the rapid release of volatile matter during high heating rate pyrolysis enhances the pore structure by increasing the pore volume and specific surface area. Further investigations are required to reveal the true nature of the increased reactivity of the HB compared to the MT char.

Table 5
Particle size information of the char residues.

	Coal A	Coal B	Coal C
HB			
d ₁₀ (μm)	3.03	2.97	3.60
d ₅₀ (μm)	18.07	14.67	16.05
d ₉₀ (μm)	96.06	78.60	40.93
MT			
d ₁₀ (μm)	3.05	3.46	2.35
d ₅₀ (μm)	17.81	16.76	11.54
d ₉₀ (μm)	113.87	87.46	38.05
NB			
d ₁₀ (μm)	3.49	4.40	3.54
d ₅₀ (μm)	20.37	18.78	15.99
d ₉₀ (μm)	92.53	59.23	42.58

3.2. Particle size distribution

The particle size distribution was measured with the Mastersizer 2000 using approximately 1 g sample. Table 5 shows the mean diameter (d₅₀), d₁₀, and d₉₀ of the different char residues.

The mean diameters follow the burnout trend at similar experimental conditions; Coal C residues have the smallest and B have the largest d₅₀. The trend is also preserved for d₁₀ and d₉₀. Moreover, a correlation between particle size and burnout ratio exists for coal A and B. Coal C yields the smallest particles for the MT experiment which has a slightly lower burnout than the HB one.

Figs. 3, 4, and 5 compare the virgin coal and experimental residue particle size distributions (PSD) and particle size sum (PSS). The particle sizes and the PSD width are reduced for all residues compared to the initial material during thermochemical conversion. Additionally, the bimodality reduces for coals A and B under all experimental conditions. The effect is most prominent for the NB cases followed by the HB cases.

Fig. 3 compares the particle size distributions of the initial coal A and the different residues. The HB and NB conditions significantly reduce the tailing peak of the initial PSD, while the tailing peak is shifted towards smaller particle sizes under MT conditions. The bimodal shape of the PSD vanishes only under NB conditions for coal A.

Fig. 4 compares the particle size distributions of the initial coal B and the different residues. During the thermochemical conversion for all experimental conditions, the bimodal shape is significantly altered towards a monomodal one. A slight tailing shoulder remains in the case of the MT residues.

Fig. 5 compares the particle size distributions of the initial coal C and the different residues. The monomodal PSD shifts towards smaller particle sizes and reduces in width under the investigated conditions. The HB and NB residues feature an almost identical PSD, while the MT residue's PSD are wider and shifted towards smaller particle sizes.

The changes in the particle size distributions give insights into the thermochemical conversion process. According to Jiménez and Ballester [28], the PSD shifts towards smaller particle sizes but keeps its shape during combustion due to the d²-law [29]. The changing PSD shapes indicate that other effects influence the PSD during the experiments. Fractionation during the dosing or sampling are two intrinsic experimental effects that are hard to verify. Particle fragmentation

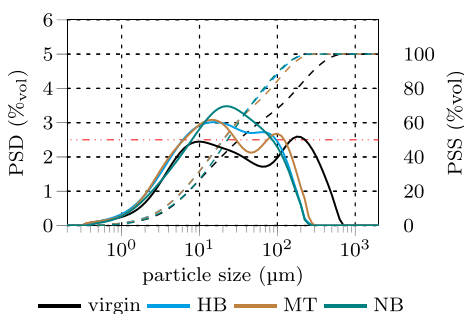


Fig. 3. Comparison of the particle size distributions (PSD) and particle size sums (PSS) of the char residues for coal A.

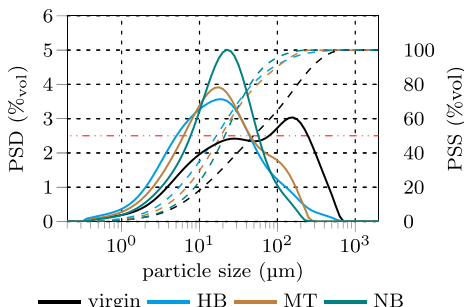


Fig. 4. Comparison of the particle size distributions (PSD) and particle size sums (PSS) of the char residues for coal B.

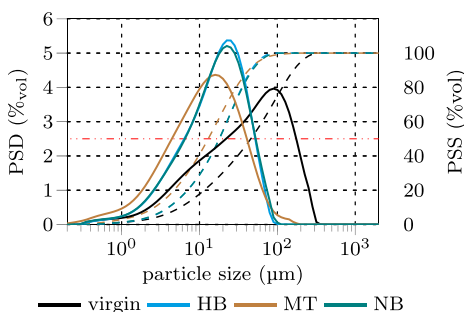


Fig. 5. Comparison of the particle size distributions (PSD) and particle size sums (PSS) of the char residues for coal C.

could also cause the PSD changes [20,28]. The reduction of the tailing peaks for coal A and B indicates particle fragmentation. Recently, Asheruddin et al. [29] experimentally observed deviations from the d^2 -law behavior, which could also be a cause for the changing PSDs. Additional investigations are required to clarify the root cause of these effects.

3.3. SEM analysis

The differences in the morphological changes during the conversion process of the HB and NB experiments are evaluated using Scanning Electron Microscopy (SEM). SEM was performed using an FEI Quanta FEG250 SEM. The particles were mounted on aluminum stubs using carbon tape and subsequently vacuum treated in a Q150T S sputter coater for 5 to 10 min at a current intensity of 15 mA. The samples were homogenized by shaking before the SEM preparation to ensure representative results.

Fig. 6 compares the virgin coal and the chars of coal A at a magnification of 20000. The virgin coal A coal has a different appearance

than coal B. It seems like deposits have been pressed to the surface during the grinding process leading to a ragged surface structure. This structure is found again in the chars' surface appearance. The NB residues have a more tidy appearance compared to the other chars and virgin coal. The tiny flakes on the char surfaces might be ash or condensed heavy pyrolysis products. Furthermore, the development of small pores is more pronounced for the HB char than for the MT and NB one. This observation is supported by the experimentally determined burnout ratios, which increase from NB via MT to HB.

Fig. 7 compares the virgin coal and the chars of coal B at a magnification of 5000. The virgin coal is dense and has smaller deposits on the surface. The SEM images show two different char particle morphologies. The NB and MT chars are low porous and show little evidence of surface attacks from oxygen or other gasification agents. In contrast, the HB char is highly porous and displays significant pore evolution caused by fixed carbon oxidation or gasification. The burnout ratios support the SEM images as the burnout increases between the NB and MT and the MT and HB conditions.

Fig. 8 compares the virgin coal and the chars of coal C at a magnification of 5000. Virgin coal C and coal B look very similar on the SEM images. The investigated char particles differ for all three experiments, nevertheless, conversion differences can be identified between them. The HB char features significantly more surface attacks and pore formation from oxidation and gasification than the MT and NB char. The depicted NB particle features a different texture than the HB one; therefore, oxidation and gasification attack boundaries between coal constituents instead of the surface. The investigated MT char residues are shell-like structures that show evidence of pore formation. Despite these differences, the HB residue is more porous than the NB one, which aligns with the experimental burnout ratios. However, the depicted MT residue deviates from this trend because of the hollow shells.

In general, the SEM images confirm the trend of the experimental burnout ratios. The residues of the NB experiments, where the particles experience lower conversion temperatures, show less indication of pore formation or pore size enlargement than the MT and HB residues.

Furthermore, the structural changes of coal B and C during the thermochemical conversion show similarities, while changes in coal A differ significantly. Coal B and C experience pore formation under all experimental conditions but to the highest extent during the HB experiments. The spherical structures are most likely melted and re-solidified ash particles deposited at the surface of the carbon matrix. These structures are less visible for coal B, which can be caused by the lower burnout and, consequently, lower heat release and reduced self-heating effects compared to coal C.

Coal A shows distinct structural changes during the conversion since the surface is covered with small flakes. These flakes are scattered on the NB and MT residues while plating the HB char carbon matrix due to re-solidification effects. The flakes are most likely ash, which is supported by a similar optical appearance as the rare spherical structures. The predominant non-spherical shape of these ash deposits indicates lower conversion temperatures for coal A than for the other coals due to reduced self-heating. Furthermore, the pore structure development is less intense compared to coal B and C.

The different structural changes are also in line with the different coal types. The (sub-)bituminous coals (B and C) tend to have higher pore formation and, consequently, higher burnout ratios than the anthracitic coal A under the investigated conversion conditions. However, there are similar conversion patterns: (i) the deposition of ash particles on the surface of the carbon structures and (ii) the formation of pores and pore structures.

4. Summary and conclusion

In this work, we present the novel Alternative Reducing Agent (ARA) Reactor, which was designed to recreate the high heating rate

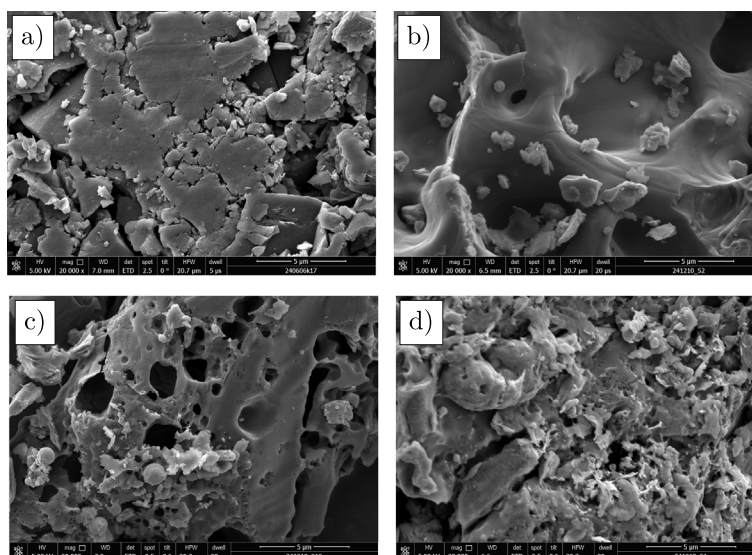


Fig. 6. SEM images of the virgin coal (a) and the NB (b), HB (c), and MT (d) residues for coal A.

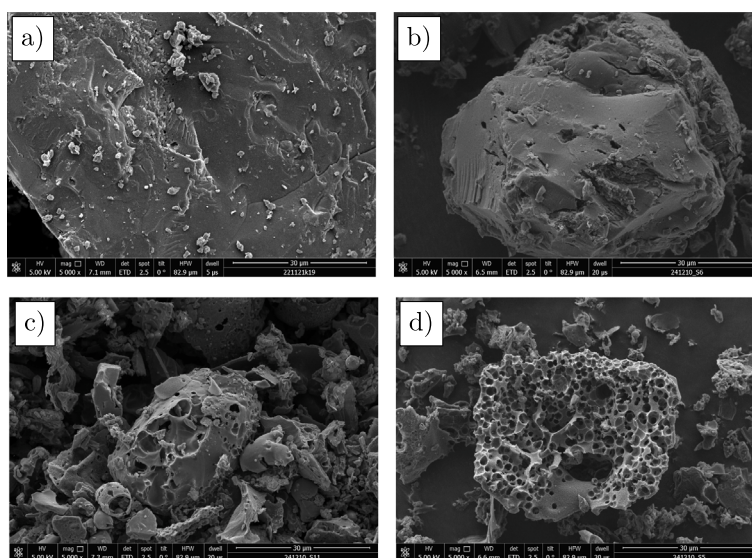


Fig. 7. SEM images of the virgin coal (a) and the NB (b), HB (c), and MT (d) residues for coal B.

conditions prevalent when injecting carbon carriers into the blast furnace raceway zone.

The thermochemical conversion characteristics at high and low heating rates of three different coals, an anthracitic, a bituminous, and a sub-bituminous, were investigated. Two different approaches were employed for the low heating rate experiments: (i) deactivation of the burner, while keeping all other settings the same (NB conditions), and (ii) deactivation of the burner while adapting the heating zone temperatures to match the exit gas phase temperature (T_{reaction}) with the corresponding high heating rate experiments (MT conditions). The experimental results indicate that the latter approach is more suitable to isolate the heating rate effect.

The experimentally determined burnout ratios resemble the coal type and are related to the volatile content: more volatiles mean increased reactivity. All coals follow the same trend for the different experimental conditions. The high heating rate condition produces slightly higher burnout ratios than the matching temperature condition, while the no burner condition gives significantly lower burnout. Despite the similar burnout of the high heating rate and matching temperature conditions, the effect of the heating rates is indicated by the share of the

solid residues, which is approximately twice as high for the matching temperature conditions as for the high heating rate ones.

Except of the heating rate, the higher water vapor concentrations in the HB cases could affect the thermochemical conversion through delayed drying or additional carbon gasification. However, we only expect marginal changes in the conversion characteristics since the vapor concentration is significantly lower than the saturation concentration and the gasification rate is typically significantly lower than the oxidation rate or the carbon dioxide gasification rate [30,31]. Although we tried to minimize differences in the effective conversion temperatures of the different experimental settings, these could also affect the conversion process. Based on the reactor settings, the MT cases could have experienced noteworthy higher temperatures compared to the other cases due to higher reaction zone temperatures. In that case, the effect of the heating rate would be under-estimated in the experimental results. The coal samples were homogenized before the experiments to avoid any influence of inhomogeneities on the conversion results. However, variations of the coal properties (porosity, macerals, proximate analysis) might also have influenced the experimental data to a minor extend. Taking into account possible influencing factors, we

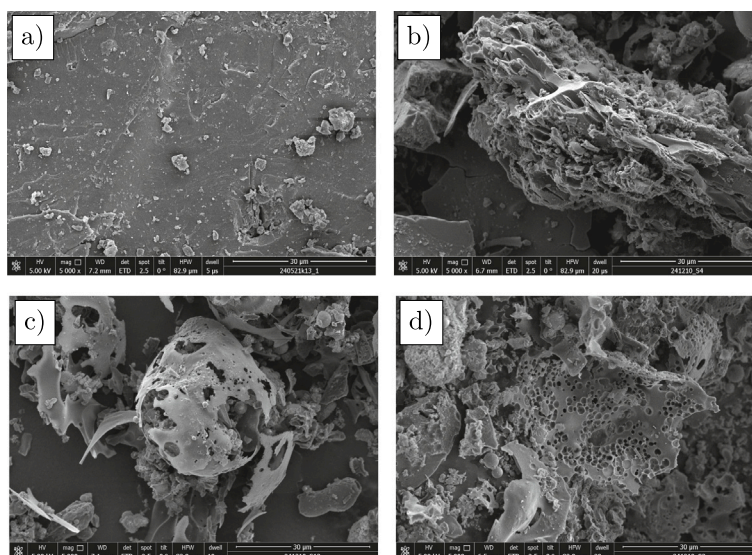


Fig. 8. SEM images of the virgin coal (a) and the NB (b), HB (c), and MT (d) residues for coal C.

are confident that we minimized their impact sufficiently to obtain meaningful results.

Particle size distributions (PSD) of the virgin coals and the experimental residues revealed PSD shape changes. The particle feeding and sampling procedure, particle fragmentation due to thermal stresses [20, 28], and deviation from d^2 -law [29] have been identified as potential causes for these changes. Additional experiments and investigations of the dosing unit confirmed the unbiased feeding of the employed revolver doser.

Scanning Electron Microscopy (SEM) of the solid residues has confirmed the different conversion characteristics of the coal types and the different experimental conditions. The bituminous and sub-bituminous coal show higher pore formation and ash melting due to self-heating from exothermic char conversion. In contrast, ash is deposited as flakes onto the char surface on the anthracitic residues.

This first attempt to experimentally investigate the effect of the heating rate on the thermochemical conversion of solid carbon carriers shows promising results. However, additional systematical investigations are required to fully understand these effects. These investigations include the variation of (i) the residence time, (ii) the reaction zone temperature, (iii) the hydrogen burner power and (iv) the hydrogen burner stoichiometry (adiabatic flame temperature). In addition the reactor state will be comprehensively modeled using a spatially resolved steady-state digital model.

CRediT authorship contribution statement

Markus Bösenhofer: Writing – review & editing, Writing – original draft, Visualization, Validation, Supervision, Software, Methodology, Data curation, Conceptualization. **Thomas Nanz:** Writing – review & editing, Visualization, Software, Methodology, Investigation, Data curation. **Hugo Stocker:** Writing – review & editing, Resources, Project administration, Funding acquisition. **Christoph Feilmayr:** Writing – review & editing, Resources, Project administration, Funding acquisition. **Johannes Rieger:** Writing – review & editing, Supervision, Resources, Project administration, Funding acquisition, Formal analysis. **Michael Harasek:** Writing – review & editing, Resources, Project administration, Funding acquisition.

Declaration of competing interest

The authors declare that they have no known competing financial interests or personal relationships that could have appeared to influence the work reported in this paper.

Acknowledgments

The authors gratefully acknowledge DI Selma Kuloglija for her assistance with the SEM measurements.

The authors acknowledge the funding support of K1-MET GmbH, whose research program is supported by COMET (Competence Center for Excellent Technologies), the Austrian program for competence centers. COMET is funded by the Austrian ministries BMIMI and BMWET, the provinces of Upper Austria, Tyrol, and Styria, and the Styrian Business Promotion Agency (SFG).

Apart from funding, the project activities are financed by the industrial partners Primetals Technologies Austria, voestalpine Stahl, voestalpine Stahl Donawitz, RHI Magnesita, and the scientific partner Technische Universität Wien.

The authors acknowledge TU Wien Bibliothek for financial support through its Open Access Funding Programme.

Data availability

Data will be made available on request.

References

- [1] D.T. Pratt, L. Smoot, D. Pratt, *Pulverized Coal Combustion and Gasification*, Springer Science & Business Media, New York, USA, 1979, <http://dx.doi.org/10.1007/978-1-4757-1696-2>.
- [2] L.D. Smoot, P.J. Smith, *Coal Combustion and Gasification*, Springer Science & Business Media, New York, USA, 1985, <http://dx.doi.org/10.1007/978-1-4757-9721-3>.
- [3] J. Szekeley, J.W. Evans, H.Y. Sohn, *Gas-Solid Reactions*, Academic Press, Cambridge, MA, USA, 1976.
- [4] C.G. Thomas, M. Shibaoka, E. Gawronski, M.E. Gosnell, D. Phong-anant, Reactive (fusible) inertinite in pulverized fuel combustion: 2. determination of reactive (fusible) inertinite, *Fuel* 72 (7) (1993) 913–919, [http://dx.doi.org/10.1016/0016-2361\(93\)90287-C](http://dx.doi.org/10.1016/0016-2361(93)90287-C).
- [5] T.K. Gale, C.H. Bartholomew, T.H. Fletcher, Effects of pyrolysis heating rate on intrinsic reactivities of coal chars, *Energy & Fuels* 10 (3) (1996) 766–775, <http://dx.doi.org/10.1021/ef950217s>.
- [6] C. Fushimi, K. Araki, Y. Yamaguchi, A. Tsutsumi, Effect of heating rate on steam gasification of biomass. 1. Reactivity of char, *Ind. Eng. Chem. Res.* 42 (17) (2003) 3922–3928, <http://dx.doi.org/10.1021/ie030056c>, [arXiv:https://doi.org/10.1021/ie030056c](https://doi.org/10.1021/ie030056c).
- [7] M. Bösenhofer, E.-M. Wartha, C. Jordan, C. Feilmayr, H. Stocker, F. Hauzenberger, J. Rieger, S. Tjaden, A. Walk, M. Harasek, Suitability of pulverised coal testing facilities for blast furnace applications, *Ironmak. Steelmak.* 47 (5) (2020) 574–585, <http://dx.doi.org/10.1080/03019233.2019.1565152>, [arXiv:https://doi.org/10.1080/03019233.2019.1565152](https://doi.org/10.1080/03019233.2019.1565152).

- [8] European Commission, Towards competitive and clean European steel, European Commission, Brussels, 2021.
- [9] C. Swalec, M. Armbruster, A. Grigsby-Schulte, Pedal to The Metal 2024: Building Momentum for Iron and Steel Decarbonization, Technical Report., Global Energy Monitor, 2024.
- [10] T. Nanz, M. Bösenhofer, J. Rieger, C. Feilmayr, F. Hauzenberger, H. Stocker, M. Harasek, A novel test rig for the evaluation of auxiliary reducing agents (ARAs), in: AISTech 2024 Proceedings, AIST, 2023, pp. 397–403, <http://dx.doi.org/10.33313/387/044>.
- [11] T. Nanz, M. Bösenhofer, J. Rieger, C. Feilmayr, H. Stocker, M. Harasek, Evaluating auxiliary reducing agents in a test rig under raceway conditions, in: AISTech 2024 Proceedings, AIST, 2024, pp. 192–200, <http://dx.doi.org/10.33313/388/024>.
- [12] M. Bösenhofer, C. Jordan, M. Harasek, C. Feilmayr, F. Hauzenberger, A. Walk, S. Tjaden, Pulverized coal injection (PCI) test facilities and methods - overview and recommendations, in: AISTech 2018 Proceedings, 2018, pp. 287–295.
- [13] M. Harasek, C. Maier, C. Jordan, M. Bösenhofer, C. Feilmayr, Investigation of alternative reducing agent conversion in the raceway cavity of blast furnaces by numerical simulation, in: AISTech - Iron and Steel Technology Conference Proceedings, 2016, pp. 353–365.
- [14] M. Bösenhofer, E.-M. Wartha, C. Jordan, F. Hauzenberger, C. Feilmayr, H. Stocker, J. Rieger, B. König, M. Harasek, Pulverized coal conversion in blast furnaces-analysis of involved scales, in: AISTech - Iron and Steel Technology Conference Proceedings, AIST, 2020, pp. 277–285, <http://dx.doi.org/10.33313/380/032>.
- [15] E.-M. Wartha, N.E. Haugen, E. Karchniwy, M. Bösenhofer, M. Harasek, T.L. as, The effect of turbulence on the conversion of coal under blast furnace raceway conditions, Fuel 331 (2023) 125840, <http://dx.doi.org/10.1016/j.fuel.2022.125840>.
- [16] M. Kiss, C. Gruber, M. Harasek, M. Bösenhofer, Modeling biomass conversion in raceway zone of blast furnace using resolved Lagrangian particle model, Energies 18 (15) (2025) 4038, <http://dx.doi.org/10.3390/en18154038>.
- [17] T.F. Wall, G. su Liu, H. wei Wu, D.G. Roberts, K.E. Benfell, S. Gupta, J.A. Lucas, D.J. Harris, The effects of pressure on coal reactions during pulverised coal combustion and gasification, Prog. Energy Combust. Sci. 28 (5) (2002) 405–433, [http://dx.doi.org/10.1016/S0360-1285\(02\)00007-2](http://dx.doi.org/10.1016/S0360-1285(02)00007-2).
- [18] H. Li, L. Elliott, H. Rogers, P. Austin, Y. Jin, T. Wall, Reactivity study of two coal chars produced in a drop-tube furnace and a pulverized coal injection rig, Energy & Fuels 26 (8) (2012) 4690–4695, <http://dx.doi.org/10.1021/ef201779q>, arXiv:<https://doi.org/10.1021/ef201779q>.
- [19] H. Li, L. Elliott, H. Rogers, T. Wall, Comparative study on the combustion performance of coals on a pilot-scale test rig simulating blast furnace pulverized coal injection and a lab-scale drop-tube furnace, Energy & Fuels 28 (1) (2014) 363–368, <http://dx.doi.org/10.1021/ef4014967>.
- [20] J.-H. Kim, R.-G. Kim, G.-B. Kim, C.-H. Jeon, Effect of coal fragmentation on PCI combustion zone in blast furnace, Exp. Therm. Fluid Sci. 79 (2016) 266–274, <http://dx.doi.org/10.1016/j.expthermflusci.2016.07.020>.
- [21] B.-H. Yan, C.-X. Cao, Y. Cheng, Y. Jin, Y. Cheng, Experimental investigation on coal devolatilization at high temperatures with different heating rates, Fuel 117 (2014) 1215–1222, <http://dx.doi.org/10.1016/j.fuel.2013.08.016>, URL <https://www.sciencedirect.com/science/article/pii/S0016236113007436>.
- [22] M. Bösenhofer, T. Nanz, M. Kiss, C. Gruber, J. Rieger, H. Stocker, C. Feilmayr, M. Harasek, Simulation-aided evaluation of alternative reducing agent conversion experiments, in: AISTech 2024 Proceedings, AIST, 2024, pp. 1838–1848, <http://dx.doi.org/10.33313/388/193>.
- [23] T. Nanz, M. Kiss, G. Zarabian, B. Weiß, M. Bösenhofer, C. Gruber, J. Rieger, C. Feilmayr, H. Stocker, M. Harasek, Towards a better understanding of ARA conversion, BHM Berg- Und Hüttenmännische Monatshefte (2025) <http://dx.doi.org/10.1007/s00501-025-01596-3>.
- [24] N. Vorobiev, Optische Untersuchung des Abbrandverhaltens von Brennstoffpartikeln in Oxyfuel-Atmosphäre [Optical investigation of the combustion behavior of fuel particles in an oxyfuel atmosphere] (Ph.D. thesis), Faculty of Mechanical Engineering at Ruhr University Bochum, 2020.
- [25] N. Gat, L.M. Cohen, A.B. Witte, R.M. Denison, Ash loss and the “seeded-tracer” technique for the determination of mass balance in rapid heating coal pyrolysis experiments, Combust. Flame 57 (3) (1984) 255–263, [http://dx.doi.org/10.1016/0010-2180\(84\)90045-2](http://dx.doi.org/10.1016/0010-2180(84)90045-2).
- [26] T.R. Ballantyne, P.J. Ashman, P.J. Mullinger, A new method for determining the conversion of low-ash coals using synthetic ash as a tracer, Fuel 84 (14) (2005) 1980–1985, <http://dx.doi.org/10.1016/j.fuel.2005.04.012>.
- [27] H. Liu, H. Zhu, L. Yan, Y. Huang, S. Kato, T. Kojima, Gasification reactivity of char with CO₂ at elevated temperatures: the effect of heating rate during pyrolysis, Asia-Pacific J. Chem. Eng. 6 (6) (2011) 905–911, <http://dx.doi.org/10.1002/apj.483>, arXiv:<https://onlinelibrary.wiley.com/doi/pdf/10.1002/apj.483>.
- [28] S. Jiménez, J. Ballester, Study of the evolution of particle size distributions and its effects on the oxidation of pulverized coal, Combust. Flame 151 (3) (2007) 482–494, <http://dx.doi.org/10.1016/j.combustflame.2007.08.001>.
- [29] N.M. Asheruddin, A.M. Shivapuji, S. Dasappa, Analysis of deviation from classical d_p^2 -law for biochar conversion in an oxygen-enriched and temperature-controlled environment, Sci. Rep. 12 (1) (2022) <http://dx.doi.org/10.1038/s41598-022-22910-w>.
- [30] D.G. Roberts, D.J. Harris, Char gasification with O₂, CO₂, and H₂O: effects of pressure on intrinsic reaction kinetics, Energy & Fuels 14 (2) (2000) 483–489, <http://dx.doi.org/10.1021/ef9901894>, URL <https://doi.org/10.1021/ef9901894>.
- [31] R. Zhang, Q.H. Wang, Z.Y. Luo, M.X. Fang, K.F. Cen, Coal char gasification in the mixture of H₂O, CO₂, H₂, and CO under pressured conditions, Energy & Fuels 28 (2) (2014) 832–839, <http://dx.doi.org/10.1021/ef4018527>.